centra
center for astrophysics and gravitation

Scientific Project

Investigating the Plasma Coupling Parameter in Low-Mass Red Giants:
Implications for Interior Structure and Impact of Metallicity

Rodrigo Ferreira Salvado

Supervisors:

Ilídio Lopes
Ana Brito

June 28, 2025

ABSTRACT

Context: Recent research by Brito & Lopes (2024) has revealed that the global stellar plasma parameter correlates with stellar rotation rates and shows significant dependence on metallicity in main sequence stars. This parameter, which quantifies the importance of electrostatic interactions within stellar interiors, could enhance our understanding of stellar evolution, particularly for evolved stars where internal structure undergoes dramatic changes. The relationship between metallicity and stellar evolution remains incompletely understood, especially in the context of electrostatic effects in stellar interiors.
Aims: To expand our understanding of stellar physics by studying the plasma coupling parameter in evolved stars, specifically low-mass red giants, with particular focus on how this parameter relates to metallicity and internal structure. This research aims to provide new insights about the relationship between electrostatic interactions and observable stellar properties.
Methods: We generated a set of twelve stellar models using the MESA stellar evolution code, covering a range of initial masses and metallicities representative of low-mass red giant stars.
Results: We found that Coulomb interactions between ions, measured by the plasma coupling parameter, are significantly stronger in the radiative core of low-mass red giants compared to the convective envelope. Our results also show that metallicity plays a key role in shaping the behavior of the plasma coupling parameter, primarily through its influence on the internal temperature profile. In the convective envelope, a clear correlation was identified between the plasma coupling parameter and the *Rosseland* mean opacity, reflecting the impact of opacity mechanisms on electrostatic interactions. Additionally, we observed a consistent metallicity ordering in the global stellar plasma parameter along nearly the entirety of the red giant branch.

I. INTRODUCTION

Stellar interiors provide a natural environment to study fundamental physical processes under extreme conditions. While much progress has been made in modeling the structure and evolution of stars, many microphysical processes that govern energy transport and particle interactions remain incompletely understood. Among these processes, electrostatic interactions, and their relation to internal structure and thermodynamical properties, may be key to better understand the physics of evolved stars, such as red giants, whose interior stratification and density profiles change dramatically after the main sequence. Recent studies by Brito & Lopes (2024) suggest that variations in metallicity significantly affect the global stellar plasma parameter, a measure of the relative strength of Coulomb interactions in stellar interiors, which is also correlated with stellar rotation rates. This work aims to investigate the plasma coupling parameter in low-mass red giants, examining how it is influenced by changes in metallicity and how it evolves along the red giant branch.

The remainder of this work is organized as follows: The study begins with a theoretical introduction that establishes the key physical concepts relevant to our analysis, including the role of electrostatic interactions in stellar interiors, the definition of the plasma coupling parameter and a brief overview on stellar evolution. Following this, the stellar models developed with the MESA code are presented, describing the physical assumptions, initial conditions, and how these low-mass red giant models were evolved up to the onset of the helium flash. We then focus on how metallicity influences the plasma coupling parameter locally. Building on this analysis, we examine how the correlation between opacity and coupling strength changes throughout the envelope. In the final part of the study, it is introduced a more global formulation of the plasma coupling parameter, which provides an integrated view of how electrostatic and thermal energies compete across the stellar evolution. The work is concluded with a discussion of the physical implications of these results and a summary of the main findings.

A. Plasma physics in stellar interiors

Plasma is a state of matter consisting of free-moving charged and neutral particles, including ions and electrons, that can occur at high temperatures or under conditions where energy is sufficient to ionize atoms. Plasma exhibits a collective behaviour and exists in various forms in nature, with each type characterized by considerable differences in temperature and electron density. Within the innermost regions of low mass stars, a hot and dense type of plasma is typically found. In this work, the focus will be particularly on this kind of plasma.

We consider two main properties of the astrophysical plasma. Plasma maintains an overall state of neutrality; however, the first property, quasi-neutrality, refers to the fluctuations in ionic density (n_i) and electronic density (n_e) at smaller scales, meaning small local imbalances of electric charge. This means that plasma exhibits some important electromagnetic properties. Due to the previously mentioned collective behavior, this implies that the motion of particles in the plasma is also influenced by the state of the plasma in distant regions. This is, the collective behavior results from the long-range effects of electromagnetic forces.

1) Debye lenght: The Debye length (λ_D) is a characteristic distance over which the Coulomb potential of

a charged particle is "screened" by the redistribution of surrounding particles with opposite charge. Numerically, the Debye length is the distance over which the potential decays to $\frac{1}{e}$ of its original value. This means that for scales larger than the Debye length, overall quasi-neutrality is maintained.

Considering the eletric potential $\Phi(r)$ of an ion of charge $+Ze$ with an electronic cloud that obeys the Poisson equation:

$$\nabla^2\Phi(r) = -4\pi\rho_e \tag{1}$$

where ρ_e is the net density of eletric charges at a given location defined by:

$$\rho_e = \sum_i n_i Z_i e - n_e e \tag{2}$$

with the ionic and electronic concentration given respectively by:

$$n_i(r) = n_{0i}\left(1 - \frac{Z_i e\Phi(r)}{kT}\right) \tag{3}$$

$$n_e(r) = n_{0e}\left(1 + \frac{e\Phi(r)}{kT}\right) \tag{4}$$

The values n_{0i} and n_{0e} represent the concentration in absence of the perturbations due to other ions or electrons, respectively, which translates to when the stellar matter in unperturbed. Finally, introducing ρ_e in the Poisson equation and assuming spherical symmetry it is possible to obtain the expression for the electrostatic potential:

$$\Phi = \frac{Ze}{r}e^{-r/\lambda_D} \tag{5}$$

where λ_D is defined by

$$\lambda_D = \sqrt{\frac{kT}{4\pi e^2\left(n_e + \sum_i n_i Z_i^2\right)}} \tag{6}$$

In stellar interiors this lenght scale represents the distance over which termal fluctuations within the stellar the material can lead to a significant separation between negatively and positively charged particles.

2) Plasma coupling parameter: From equation 6 one can easily see how the Debye lenght relates to the net density and the thermal kinetic energy, kT. Therefore, the characteristics of the stellar plasma will be influenced by the electrostatic potential energy and the thermal energy of the particles within the star.

The plasma coupling parameter, represented by Γ_i, consists of a ratio of Coulomb potential energy to the thermal energy, that is used to characterize the electrostatic properties of stellar interiors and it is defined as

$$\Gamma_i = \frac{(\overline{Z_i}e)^2}{a_i kT} \tag{7}$$

where the Wigner–Steitz radius a_i, that represents the mean inter-ion distance, is given by:

$$a_i = \left(\frac{3\overline{Z_i}}{4\pi n_e}\right)^{1/3} \tag{8}$$

The higher the value of the plasma coupling parameter, the more significant the Coulomb interactions between ions become. Also, as the Coulomb and thermal energies approach balance, the plasma coupling parameter approaches unity. For cases where the plasma coupling parameter is greater than one, electrostatic interactions dominate, and the plasma becomes more strongly coupled. This corresponds to a smaller Debye length, indicating that charge imbalances are neutralized over shorter distances, and the Coulomb interactions are more pronounced. On the other hand, if this value is much lower than one, it indicates that thermal energy dominates over electrostatic interactions. In this case, the plasma is considered weakly coupled, with a behavior primarily influenced by the kinetic motion of the particles rather than their electrostatic interactions. [1] [6]

Despite the plasma coupling parameter being a local variable, we can define a new parameter, the global stellar plasma parameter, which has a global character:

$$\overline{\Gamma} = \frac{1}{M}\int_0^M \Gamma_i\, dM(r), \tag{9}$$

where

$$dM(r) = 4\pi r^2\rho\, dr, \tag{10}$$

Generally, the greater the value of $\overline{\Gamma}$, the more significant are the Coulomb interactions for the star as a whole. [3]

3) Opacity: The opacity of stellar matter determines the speed at which a star spends its energy, governing how radiation is transported through the stellar interior. It quantifies the resistance that matter offers to the flow of radiation and directly affects the temperature gradient and energy transport mechanisms within a star. The opacity at any given point depends on several local properties, including density, temperature, and chemical composition. In stellar interiors, photons interact with matter through several processes such as bound-bound transitions (absorption or emission between atomic energy levels), bound-free absorption (photoionization), free-free absorption (bremsstrahlung), and scattering. The relative importance of these processes varies with the local physical conditions.

Due to the highly varying nature of opacity with frequency, it is not practical to work with the monochromatic opacity κ_ν at every point in the spectrum. Instead, an average opacity is used. In the context of this work the appropriate averaging is given by the *Rosseland* mean opacity, defined as:

$$\frac{1}{\kappa_R} = \frac{\int_0^\infty \frac{1}{\kappa_\nu}\frac{\partial B_\nu}{\partial T}\, d\nu}{\int_0^\infty \frac{\partial B_\nu}{\partial T}\, d\nu}, \tag{11}$$

where κ_ν is the monochromatic opacity at frequency ν and the weighting function is the partial derivative of the Planck function with respect to the temperature. [8] [9]

B. Stellar Evolution of Low-Mass Stars

During the main sequence phase, low-mass stars burn hydrogen in their cores via the proton-proton (pp) chain, maintaining hydrostatic equilibrium. This phase constitutes the longest period of stellar evolution, where the star remains relatively stable in both luminosity and effective temperature.

1) The Schönberg–Chandrasekhar limit: At a certain point in time, the isothermal core is not capable of supporting the material above it due to its mass increment. Therefore, there is a maximum fraction of a star's mass that can exist in said core while maintaining hydrostatic equilibrium. This was estimated by M.Schönberg and Chandrasekhar and is given by

$$\left(\frac{M_{\text{ic}}}{M}\right)_{SC} \approx 0.37 \left(\frac{\mu_{\text{env}}}{\mu_{\text{ic}}}\right)^2, \tag{12}$$

where μ_{env} and μ_{ic} are, respectively, the mean molecular weights of the overlying envelope and the isothermal core.

Nonetheless, the mass of the core may exceed this limit if an additional pressure source can supplement the ideal gas pressure. This occurs if the electrons start to become degenerate due to the increasing density of the gas, forcing electrons to occupy the lowest available energy levels. However, electrons are fermions so quantum mechanics, specifically the Pauli exclusion principle, dictates that they can't all occupy the same quantum state which results in degeneracy pressure making it possible to surpass the Schönberg–Chandrasekhar limit. [4]

2) Post-Main Sequence Evolution of Low-Mass Stars: Stars with lower masses, usually with $M < 2.3M_\odot$, evolve in distinct ways (when compared to higher-mass stars) after the exhaustion of hydrogen in the central region of the core. This type of main-sequence stars has either small or no convective cores, the latter being the case for stars with a mass around $1M_\odot$. This means that there is a smooth transition from central to shell hydrogen burning.

The end of the main-sequence phase of evolution occurs when the hydrogen burning ceases in the star's core. The star enters then the called subgiant branch, as the shell continues to consume the hydrogen available at the base of the envelope. As this process progresses, the helium core steadily grows, becoming nearly isothermal. At this stage, the Schönberg–Chandrasekhar limit is reached, and the core begins to contract rapidly. The gravitational energy released by this contraction causes the envelope to expand, while the effective temperature decreases and luminosity increases, leading to the star's redward evolution on the HR diagram.

The decrease in temperature in the envelope will promote the formation of the H^- ion, which, upon interacting with photons, absorbs them through a bound-free transition, thereby increasing the photospheric opacity. The result is the development of a convection zone near the surface, with a tendency to extend deeper into the star's interior over time, increasing the efficiency of energy transport to the surface. As a consequencce of these processes, the star rapidly ascends along the red giant branch (RGB) of the HR diagram. When the convection zone deepens and reaches regions where the chemical composition has been modified by nuclear processes, the processed material is mixed with the overlying layers, a process known as the first dredge-up, which will altere the chemical composition of the photosphere.

At the tip of the RGB, the temperature increases and pushes the hydrogen shell outward while the helium core is collapsing, becoming strongly electron degenerate. The next event is the helium flash, a rapid ignition of helium fusion in the degenerate core. However, due to its extremely short duration and the complex, dynamic changes it induces, the helium flash phase will not be discussed in this work. Modeling it accurately requires extremely small time steps, making it computationally intensive and challenging to follow in detail. [4] [5]

II. MESA SIMULATIONS

In this project, the Modules for Experiments in Stellar Evolution (MESA) was used. MESA is designed to evolve stellar models by integrating the coupled system of differential equations that describe stellar structure and composition changes over time. Basically, at each time step, MESA assembles and solves the matrix of finite-difference equations, that include the ones enumerated below:

$$\textbf{Mass Conservation:} \quad \frac{dr}{dm} = \frac{1}{4\pi r^2 \rho}, \tag{13}$$

where $\boldsymbol{r}$ represents the radius from the star's center, $\boldsymbol{m}$ is the mass within the radius and $\boldsymbol{\rho}$ is the local density.

$$\textbf{Hydrostatic Equilibrium:} \quad \frac{dP}{dm} = -\frac{Gm}{4\pi r^4}, \tag{14}$$

where $\boldsymbol{P}$ is the pressure and $\boldsymbol{G}$ is the gravitational constant.

$$\textbf{Energy Generation:} \quad \frac{dL}{dm} = \varepsilon \tag{15}$$

where $\boldsymbol{\varepsilon}$ is the energy generation rate per unit mass.

$$\textbf{Radiative Transport:} \quad \frac{dT}{dm} = -\frac{3\kappa L}{256\pi^2 a c r^4 T^3}, \tag{16}$$

where $\boldsymbol{T}$ is the local temperature, $\boldsymbol{\kappa}$ refers to the Rosseland mean opacity, $\boldsymbol{a}$ is the radiative constant and $\boldsymbol{c}$ is defined as the speed of light in vaccum, as usual.

$$\textbf{Convective Transport:} \quad \frac{dT}{dm} \approx \frac{T}{P}\frac{dP}{dm}\nabla_{\text{ad}}, \tag{17}$$

where $\nabla_{\text{ad}} \equiv \left(\frac{d\ln T}{d\ln P}\right)_{\text{ad}}$ is the adiabatic temperature gradient, which describes how the temperature changes with pressure under adiabatic conditions.

In addition to the five structure equations presented above, MESA requires a set of auxiliary relations in order to close the system of stellar evolution equations. These include the equation of state, $P = P(\rho, T, \{X_i\})$ and $\rho = \rho(P, T, \{X_i\})$. MESA also relies on opacity tables that provide $\kappa = \kappa(\rho, T, \{X_i\})$ and nuclear energy generation rates. These are usually given as two separate terms: ε_{nuc}, representing the total nuclear energy released per unit mass, and ε_ν, which accounts for the fraction of that energy lost via neutrinos and thus not available to heat the star.

Furthermore, the chemical composition is not static and evolves over time due to nuclear reactions and mixing processes. The time evolution of the mass fraction X_i of each isotope i is governed by:

$$\frac{\partial X_i}{\partial t} = \frac{\rho}{m_i}\left(j\sum r_{ji} - k\sum r_{ik}\right) + \text{mixing terms} \tag{18}$$

where $\boldsymbol{X_i}$ is the mass fraction of isotope i, $\boldsymbol{r_{ji}}$ is the reaction rate producing isotope i from isotope j and $\boldsymbol{m_i}$ is the atomic mass of isotope i; It is worth mentioning that the mixing terms include processes such as convection, overshooting, rotational mixing, and diffusion, depending on the physics enabled in the simulation.

All variables and functions introduced in these equations must be properly described and defined in the text. Together, these relations ensure that the model accounts not only for the mechanical and thermal structure of the star, but also for its evolving composition and energy generation through nuclear burning. [7]

In this work, using, specifically, the *1M_pre_ms_to_wd* test-suite to model the evolution of low mass-stars, specifically, with initial masses extending from 1.1 to 1.5 $M_\odot$. We will focus on modeling the evolution from the pre-main sequence phase up to the onset of the helium flash by using 3 of the inlists of this test-suite: *inlist_start*, *inlist_to_end_core_h_burn* and *inlist_to_start_he_core_flash*. We used MESA version 24.08.1 and the code was then compiled using MESA SDK version 24.7.1.

Twelve stellar models were developed with initial masses of 1.1, 1.3, and 1.5$M_\odot$. For each mass, four models were computed with metallicities ranging from $Z = 0.01$ to $Z = 0.04$. The end of the main sequence was defined by the mass fraction of hydrogen in the stellar core. When it drops below 0.0001, core hydrogen burning is considered complete, marking the transition to the subgiant branch. At this point, the next inlist takes over to continue until helium flash takes place. Other relevant properties of the model include the absence of rotation, implying that angular momentum transport is neglected, and the use of the Reimers mass loss prescription, a commonly adopted formulation for red giants. [2]

A Hertzsprung–Russell (HR) diagram, that displays the relationship between a star's luminosity and its effective temperature was constructed to provide a visual framework of the actual evolutionary stage of our models, as shown in Figure 1.

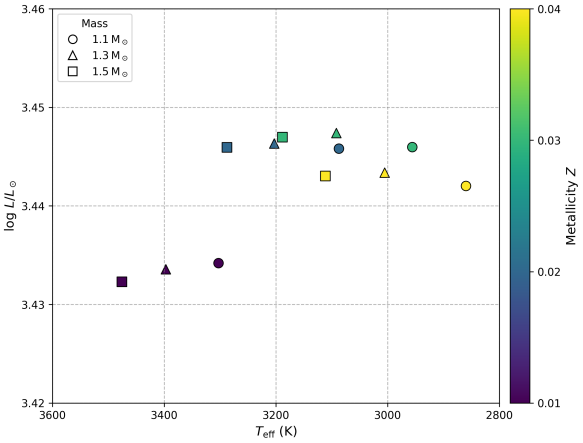

Fig. 1: Hertzsprung–Russell diagram of the stellar models developed. The shape of each point represents the initial stellar mass, while the color indicates the metallicity, as shown in the legend.

III. The Plasma Coupling Parameter in Low-Mass Stars

A. *Analyzing how the physics in stellar interiors influence* Γ_i

The plasma coupling parameter, introduced by equation 7 is a measure of the influence of electrostatic effects in stellar interiors. Figure 2 displays this parameter plotted for 3 stars with different masses and initial metallicity of $Z = 0.02$ in a stage of evolution just preceding helium flash.

Analysing the 3 images we can easily see that for this range of masses the behaviour of the plasma coupling parameter is quite similar. First, each model displays a radiative core (shaded in blue), and notably, the core masses are similar across all the cases, which means the mass increment from one model to another affects only the convection zone.

In the radiative core, Γ_i is significantly bigger than in the convective zone. This fact reflects the core's physical conditions since its extremely high density and pressure means electronic density outweighs temperature effects, producing higher values of Γ_i than in much cooler regions, such as the outer convective

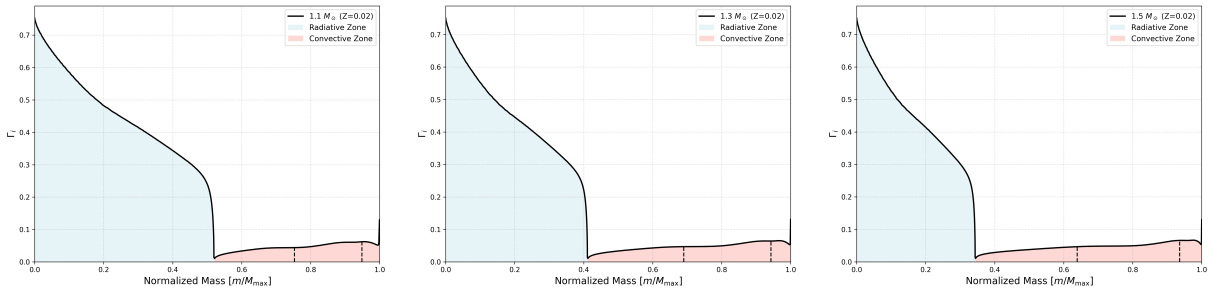

Fig. 2: Plasma coupling parameter, Γ_i, for three stellar models of different masses with a metalicity of $Z = 0.02$, as a function of the fractional mass. The images show models at the stage immediately preceding the helium flash, meaning they all represent the same evolutionary phase, despite the clear differences in age (2840.15 Myr, 4683.88 Myr and 8619.97 Myr, respectively). The dotted lines divide three regions of equal lenght in radius for better understanding of how the mass increases in comparison with the radius. Radiative and convective zones are shaded in the color blue and light red, respectively.

zone. Therefore, even though electrostatic interactions do not dominate over thermal energies, the influence of Coulomb interactions remains highly significant in this region. In fact, if we take equation 7 and we plug in the expression 8 we get:

$$\Gamma_i = \frac{(\overline{Z_i})^{\frac{5}{3}} e^2 (4\pi n_e)^{\frac{1}{3}}}{3^{\frac{1}{3}} kT} \tag{19}$$

From this we can deeeply analyse the Γ_i behaviour inside the star. Firstly, as shown in Figure 3, for all models both the ratio $\frac{n_e^{1/3}}{T}$ and our approximation for the mean ionic charge, $\bar{Z}_i$, undergo a pronounced decline when crossing from the radiative core into the convective envelope.

The drop in the mean ionic charge reflects the change from a helium-rich core, where fully ionized He nuclei contribute with two electrons per ion, to a hydrogen-rich convective envelope—where each H nucleus contributes with only one electron per ion. It is also worth noting that in corresponding regions of the stars $\bar{Z}_i$ is approximately the same across these models, which goes according with the predicted theory since the metallicity is the same, which later, in this work, will not be the case. On the other hand, while the core is strongly electron degenerate and has temperatures of around $10^8 K$, in the inner convective envelope, the temperature drops dramatically at the frontier and keeps dropping at a steady pace (temperature gradient needed to drive convection is shallower). In this region, Z_i remains approximately constant. Despite the drop in the electronic density, n_e, we observe a slight increase in the coupling parameter, Γ_i, starting at the base of the convective zone. This behavior suggests that the increase in Γ_i is primarily driven by the temperature, making it the dominant factor in this zone.

One can also conclude that, in this stage of stellar evolution and for this range of masses, the overall behaviour of Γ_i is not affected in a significant way by mass changes.

B. Dependence of the local plasma coupling parameter on metallicity

The next phase of this study examines the impact of changes in the metallicity, Z, on the plasma coupling parameter in the various stellar regions. We hold the initial mass fixed at $M = 1.5\, M_\odot$ and stop the evolution of our model at the tip of the RGB. Figure 4 shows the profiles of Γ_i for four different metallicities and table I shows some additional characteristics of the models.

Metallicity	Age [Myr]	Total mass [$M_\odot$]	Core's Mass [$M_\odot$]
$Z = 0.01$	2399.14	1.383	0.480
$Z = 0.02$	2840.15	1.375	0.474
$Z = 0.03$	3022.06	1.376	0.468
$Z = 0.04$	3012.93	1.379	0.463

TABLE I: Stellar model properties at the tip of the RGB for the four different metallicities.

Analyzing Figure 4 and table I , we observe that in the inner radiative core, higher metallicity initially corresponds to a larger plasma coupling parameter. However, this trend does not persist throughout the core, as the coupling parameter decreases more rapidly for higher-metallicity models, which have associated a smaller core mass. Due to the radiative nature of the core, where the temperature gradient is governed by equation 16, and quantum effects cannot be neglected since $\frac{E_f}{k_B T} \gg 1$, the resulting behavior becomes highly unpredictable and significantly harder to track and model compared to, for example, a convective core where such quantum effects are absent.

Before analyzing how Γ_i varies with metallicity, Z, in the convective envelope, it is important to analyze the local metallicity distribution throughout the star for the 4 different initial metalicities. This can be seen in Figure 5 and clearly cannot be considered a valid explanation for the variations in Γ_i, as it remains practically constant across the models and the profiles never come close to intersecting. Therefore, we can rule out the hypothesis that differences in local metallicity are directly responsible for the increases or decreases

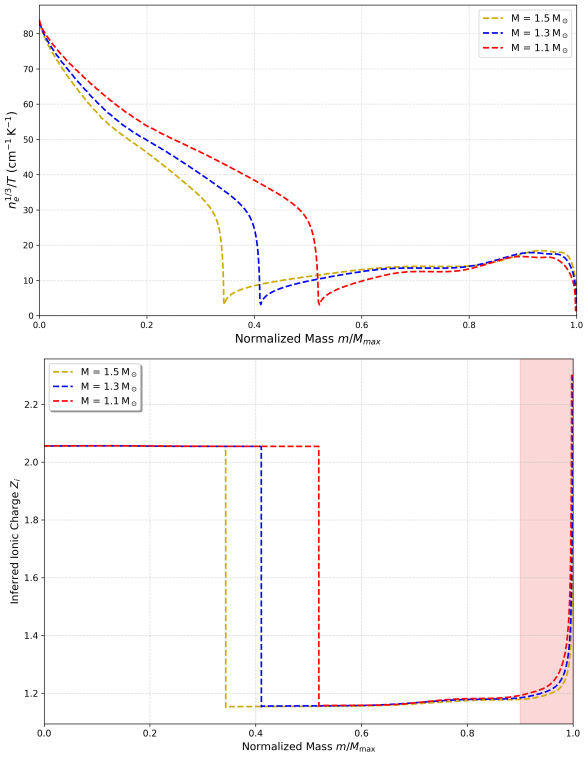

Fig. 3: The $\frac{n_e^{1/3}}{T}$ ratio and the mean ionic charge $\bar{Z}_i$ as a function of the normalized mass. It is worth noting that MESA does not directly output the mean ionic charge; the approximation we used for $\bar{Z}_i$ was inferred by isolating the corresponding variable in equation 19. For the outermost layers, where $m/M_{\rm max} > 0.9$ (shaded in red), this approximation progressively loses physical significance and should no longer be regarded as reliable.

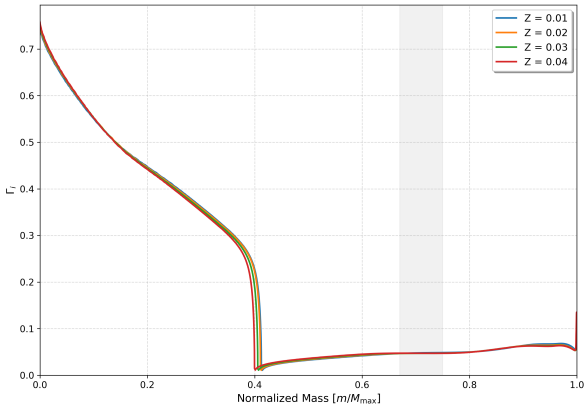

Fig. 4: Ionic plasma coupling parameter Γ_i as a function of normalized internal mass for four stellar models with metallicities extending from $Z = 0.01$ up to $Z = 0.04$. The lightgray area highlights the inversion in the metalicity trend, in the convective envelope.

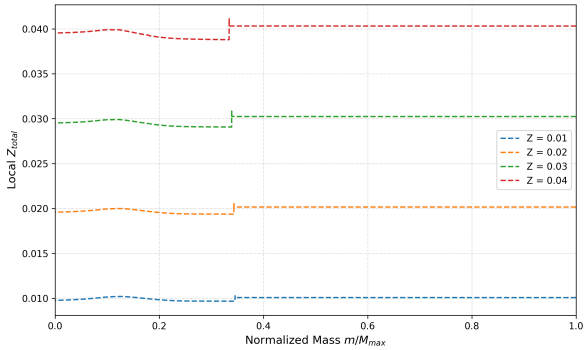

Fig. 5: Local total metal mass fraction $Z_{\rm total}$ as a function of normalized mass m/M_{max} for four initial metallicities (for an initial mass of 1.5 $M_\odot$). The atoms of carbon, nitrogen, and oxygen are the primary contributors to this value.

in the local plasma coupling parameter for this models with different total metallicity.

A closer inspection of the graph reveals that in the inner convective envelope, extending from the base of the envelope up to approximately a normalized mass of 0.7, there is a subtle but consistent trend: higher metallicity (Z) is associated with higher values of Γ_i, indicating a greater degree of plasma coupling. Although the curves appear to nearly intersect, this trend suggests that electrostatic interactions are slightly more pronounced in higher-Z models within this region. Beyond this threshold, however, the trend reverses: lower metallicity models exhibit higher values of Γ_i, implying that Coulomb interactions become relatively more significant in the outermost layers.

We can also plot the *Rosseland mean opacity*, κ_R, defined by equation 11.

The graph shown in Figure 6 reveals an interesting correlation between the opacity and the plasma coupling parameter. In the inner envelope, extending up to approximately 70% of the total mass, the opacity is higher for models with a larger CNO mass fraction.

In this region, where the temperature is still close to 10^5 K, the dominant source of opacity is metal ionization, primarily through bound-free transitions involving partially ionized elements such as C,N and 0. Since models with higher metallicity exhibit lower temperatures due to enhanced line cooling, they remain within the regime where metals are still partially ionized and actively contribute to the opacity. [10] As a result, higher metallicity leads to higher opacity in this temperature range, consistent with theoretical expectations. For temperatures above approximately 1–2 $\times$ 10^4 K, the opacity can be approximated by:

$$\kappa \simeq \kappa_0 \, \rho \, T^{-3.5} \tag{20}$$

However, beyond this point, where the temperature continues to decrease in the outer envelope, we observe an inversion in this trend, with lower metallicity models exhibiting higher opacity values. This reflects the startin-gof a shift in the dominant opacity mechanism, as the contribution from H^- absorption becomes increasingly

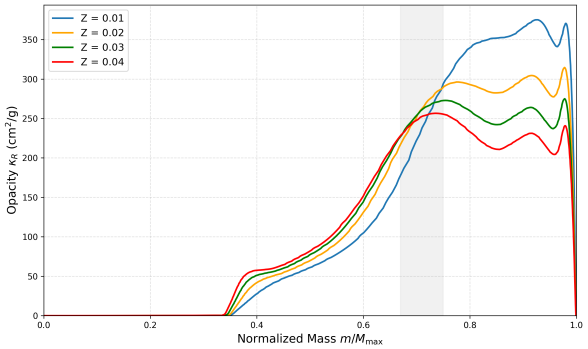

Fig. 6: Rosseland mean opacity, κ_R, as a function of normalized internal mass for four stellar models with metallicities extending from $Z = 0.01$ up to $Z = 0.04$. The lightgray area highlights the inversion in the opacity trend.

important. The formation of H^-, which requires both neutral hydrogen atoms and free electrons, is strongly temperature dependent and its opacity contribution is approximately proportional to:

$$\kappa_{H^-} \sim \rho^{0.5} T^9 \quad cm^2 g^{-1} \tag{21}$$

Finally, we reach the correlation we want to highlight, which reveals to be true for all stellar masses that we simulated in this work. In the convective envelope, we can analyse the relative impact of the metallicity in the plasma coupling parameter by looking at the mean opacity profile. We found that regions where higher metallicity leads to higher opacity also correspond to higher values of Γ_i, indicating stronger electrostatic interactions. Conversely, in regions where higher metallicity results in lower opacity due to enhanced radiative cooling and reduced ionization the plasma coupling parameter is also lower. This direct correlation between opacity and Γ_i reinforces the idea that temperature, modulated by metallicity through opacity, plays a central role in determining the strength of Coulomb interactions in the stellar envelope of red giants.

C. Dependence of the global plasma coupling parameter on age after the MS

As discussed in the theoretical introduction, there exists a parameter that characterizes the global balance between electrostatic and thermal energies within the star. Figure 8 represents the evolution of the global plasma parameter, $\overline{\Gamma}$, given by equation 9, throughout the time after the end of the main sequence up until the point just before the helium flash. Time has been normalized so that $t = 0$ corresponds to the terminal point of the main sequence and $t = 1$ to the profile immediately preceding the helium flash. We will use four different metalicities, from $Z = 0.01$ to $Z = 0.04$, and three values for the initial mass, 1.1, 1.3 and 1.5 $M_\odot$.

Examining these graphs we can see that up to a certain point in time, greater than $t = 0.8$, there is a an

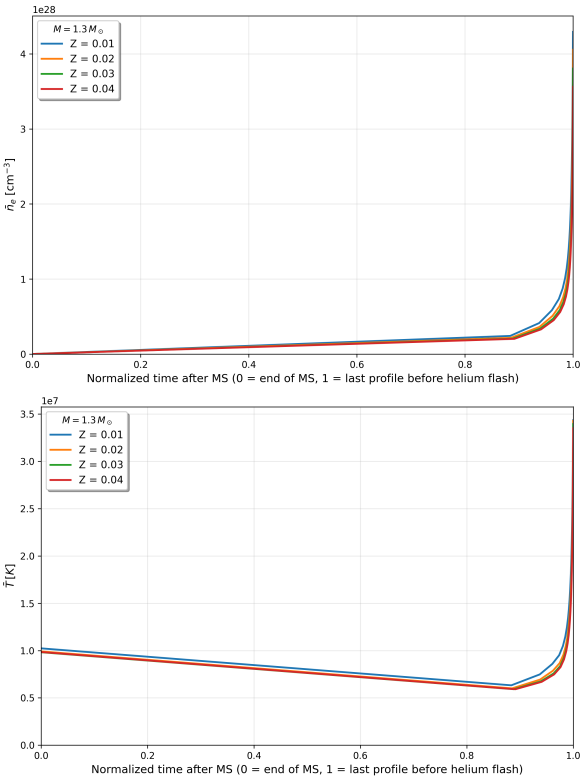

Fig. 7: Mean eletronic density ($\bar{n}_e$) and mean temperature ($\bar{T}$) as a function of normalized age after the main sequence up until the helium flash.

almost linear growth of this parameter. This behavior reflects the gradual contraction of the stellar envelope and core after core hydrogen exhaustion. As the mean density increases and the average temperature declines, Coulomb interactions become progressively stronger throughout the star. We also observe a clear metallicity ordering, where models with higher metallicity, Z, exhibit systematically higher values of the global plasma coupling parameter, $\bar{\Gamma}$, suggesting that electrostatic interactions play a more significant role in stellar structure at this evolutionary stage when the metallicity is higher.

This approximately linear trend holds throughout most of the evolution, until the final stages of the timeline, where both the mean electronic density, equation 22, and the mean temperature, equation 23, increase rapidly, following an exponential behaviour, as illustrated in Figure 7, for the case of the $1.3\,M_\odot$ model.

$$\bar{n}_e = \frac{1}{M} \int_0^M n_e \, dM(r) \tag{22}$$

$$\bar{T} = \frac{1}{M} \int_0^M T \, dM(r) \tag{23}$$

This is consistent with theoretical expectations since during the late red giant branch (RGB) phase, the

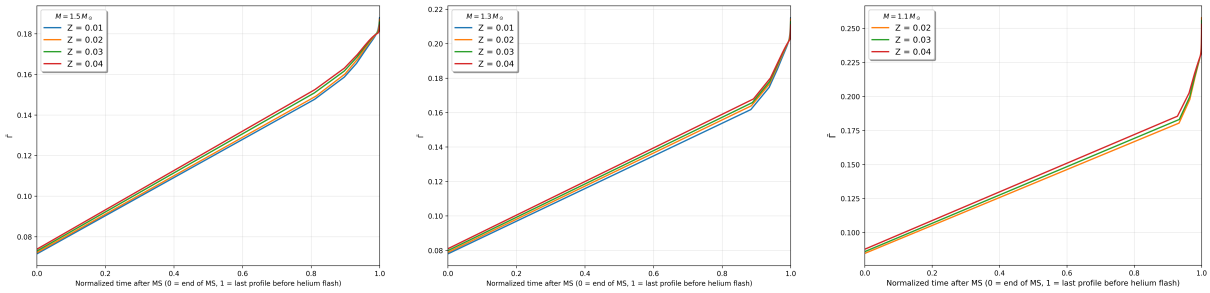

Fig. 8: Global plasma parameter, $\overline{\Gamma}$, as a function of age for four values of metalicity and for 3 different masses. The time on the x-axis is normalized and goes from the end of the main sequence to the start of helium flash for each one of the models. The model with $1.1\,M_{\odot}$ and $Z = 0.01$ is excluded from the discussion, as it exhibits markedly different behaviour compared to the other models.

helium core contracts, leading to a significant rise in both temperature and pressure. Despite this increase in both mean temperature, $\bar{T}$, and mean electronic density, $\bar{n}_e$, the global plasma coupling parameter follows the behavior of $\bar{n}_e$. Since the core encompasses roughly 40% of the stellar mass, in the case of the $1.3\,M_{\odot}$ model, the growing contribution of n_e to the mass-weighted integrals its what drives $\bar{\Gamma}$ to increase more sharply.

This causes the metallicity dependent trends to also break down in the late stages , reflecting the increasingly unstable thermodynamical behaviour of the core.

IV. Conclusions

Conclusion

Summarizing, this study aimed to investigate how the plasma coupling parameter, Γ_i, varies across the interior of low-mass red giant stars, and how this variation is influenced by metallicity and opacity. Using twelve MESA models with masses of 1.1, 1.3, and 1.5$M_{\odot}$ and metallicities ranging from $Z = 0.01$ to $Z = 0.04$, we systematically analyzed the physical conditions leading to changes in Γ_i.

In the first part of Chapter III, we explored the inner profiles of Γ_i for the models with different masses, for metallicity $Z = 0.02$, in the moments preceding the helium flash. In the radiative core, the plasma coupling parameter, Γ_i, reaches peak values exceeding 0.7, significantly higher than in the convective envelope, where it remains below $\Gamma_i = 0.15$. A sharp decrease in Γ_i is observed at the boundary between these regions, indicating a rapid drop in both electronic density and temperature. We also concluded that, within the convective envelope, the dominant factor influencing Γ_i is the steady decline in temperature. Finally, by comparing the models shown in Figure 2, we find that the overall behavior of Γ_i remains, in overall, qualitatively unchanged, suggesting that is largely independent of stellar mass in this regime.

In section III-B, figure 4, it was observed that in the radiative core, higher metallicity initially leads to a higher Γ_i, but this trend quickly vanishes due to the smaller core mass associated with higher Z. In the analysis of the convective envelope, we identified two distinct regimes. For normalized mass values below approximately 0.7, higher metallicity models exhibit higher values of Γ_i, indicating relatively stronger Coulomb interactions compared to the lower-metallicity counterparts in these inner regions. This trend inverts beyond the value previously mentioned, where lower metallicity models begin to display higher Γ_i, suggesting that electrostatic interactions become comparatively more relevant in the outer layers of those models. This inversion was further analyzed using the Rosseland mean opacity profile, figure 4. We found that opacity follows the same trend: initially increasing with Z up to $m/M_{max} \approx 0.7$, then decreasing for higher metallicity in the outer envelope. This behavior can be explained by the temperature dependence of the dominant opacity mechanisms in each region, as described by equations 20 and 21, as well as by the enhanced line cooling present in high-metallicity models. We conclude that in the convective envelope, the relative impact of metallicity on the plasma coupling parameter can be assessed by examining how it correlates with the mean opacity profile.

Finally, we introduced a global version of the plasma coupling parameter to evaluate the overall balance between thermal and electrostatic energies. We analyzed how this parameter evolves from the end of the main sequence up to the onset of the helium flash, and found that it consistently follows a metallicity ordering: Models with higher metallicity exhibit higher global values of the coupling parameter throughout the most of the evolutionary track.

Together, these results clarify how metallicity modulates the plasma coupling both locally and globally, through its impact on opacity and temperature structure. In this initial study, we focused on a set of non-rotating, low-mass red giant models. However, given the established correlation between stellar rotation and the global plasma coupling parameter in previous studies,

it would be interesting to explore this relationship in a future work.

ACKNOWLEDGMENTS

I would like to thank my mentors, Prof. Ilídio Lopes and Prof. Ana Brito, for all the help, guidance, and support throughout this work. I'm also really grateful to Diogo Capelo and João Vasconcelos for the help and advices which made learning how to work with MESA much easier.

REFERENCES

[1] A. Maeder, *Physics, Formation and Evolution of Rotating Stars*, Springer, 2010, Astronomy and Astrophysics Library.

[2] M. Cantiello, C. Mankovich, L. Bildsten, J. Christensen-Dalsgaard, and B. Paxton, "Angular Momentum Transport within Evolved Low-Mass Stars," *Astrophysical Journal*, 2014, doi: 10.1088/0004-637X/789/2/130.

[3] A. Brito and I. Lopes, "A study of the electrostatic properties of the interiors of low-mass stars: Possible implications for the observed rotational properties," *Astronomy and Astrophysics*, vol. 690, A228, 2024, doi: 10.1051/0004-6361/202450670.

[4] B. W. Carroll and D. A. Ostlie, *An Introduction to Modern Astrophysics*, 2nd ed., Pearson Education Limited, 2014.

[5] R. Kippenhahn, A. Weigert, and A. Weiss, *Stellar Structure and Evolution*, 2nd ed., Springer, Astronomy and Astrophysics Library, 2012.

[6] MIT Plasma Science and Fusion Center, *Official Website*, https://www.psfc.mit.edu/

[7] Modules for Experiments in Stellar Astrophysics, *MESA Documentation*, https://docs.mesastar.org/

[8] M. T. Lederer and B. Aringer, *Low temperature Rosseland opacities with varied abundances of carbon and nitrogen*, doi: 10.1051/0004-6361:200810576. Available at: https://www.aanda.org/articles/aa/pdf/2009/04/aa10576-08.pdf

[9] M. Pettini *Structure and Evolution of Stars — Lecture 5*

[10] D. R. Alexander and J. W. Ferguson, *Low-temperature Rosseland opacities*, doi: 10.1086/175039